 ©2001 Uspekhi Fizicheskikh Nauk, Russian Academy of Sciences

CONFERENCES AND SYMPOSIA

PACS number: 01.10.Fv

Scientific session of the Division of General Physics and Astronomy of the Russian Academy of Sciences (30 May 2001)

A scientific session of the Division of General Physics and Astronomy of the Russian Academy of Sciences (RAS) was held on May 30, 2001 at the P N Lebedev Physics Institute, RAS. The following reports were presented at the session:

(1) **Vdovin E E, Khanin Yu N, Dubrovskiĭ Yu V** (Institute of Microelectronics Technology and High-Purity Materials, RAS, Moscow region, Chernogolovka), **Veretennikov A** (Institute of Solid-State Physics, RAS, Moscow region, Chernogolovka), **Levin A, Patane A, Eaves L, Main P C, Henini M** (The School of Physics and Astronomy, University of Nottingham, Nottingham, UK), **Hill G** (Department of Electronic and Electrical Engineering, University of Sheffield, Sheffield, UK) "Magnetotunneling spectroscopy imaging of electron wave functions in self-assembled InAs quantum dots";

(2) **Volkov V A, Takhtamirov É** (Institute of Radio Engineering and Electronics, RAS, Moscow), **Ivanov D Yu, Dubrovskiĭ Yu V** (Institute of Microelectronics Technology and High-Purity Materials, RAS, Moscow region, Chernogolovka), **Eaves L, Main P C, Henini M** (The School of Physics and Astronomy, University of Nottingham, Nottingham, UK), **Maude D K** (Grenoble High Magnetic Field Laboratory, MPI-CNRS, France), **Portal J-C** (Grenoble High Magnetic Field Laboratory, MPI-CNRS, Institut Universitaire de France, and Institut National des Sciences Appliquées, Toulouse, France), **Maan J C** (High Field Magnet Laboratory, Research Institute for Materials, University of Nijmegen, The Netherlands), **Hill G** (Department of Electronic and Electrical Engineering, University of Sheffield, Sheffield, UK) "Tunneling spectroscopy of quasi-two-dimensional plasmons";

(3) **Dvurechenskiĭ A V, Yakimov A I** (Institute of Semiconductor Physics, Siberian Branch of the Russian Academy of Sciences, Novosibirsk) "Quantum dot Ge/Si heterostructures";

(4) **Lozovik Yu E** (Institute of Spectroscopy, RAS, Moscow region, Troitsk) "Exciton Bose condensate control and the phonon laser";

(5) **Subashiev A V** (State Technical University, St.-Petersburg) "Effective polarized electron emitters based on semiconductor nanostructures".

An abridged version of these reports is given below.

Uspekhi Fizicheskikh Nauk **171** (12) 1365 – 1379 (2001)
Translated by E Yankovsky; edited by A Radzig

PACS numbers: **71.24.+q**, 73.40.Gk, 73.61.Ey, 73.61.Tm
DOI: 10.1070/PU2001v044n12ABEH001055

Magnetotunneling spectroscopy imaging of electron wave functions in self-assembled InAs quantum dots

E E Vdovin, Yu N Khanin, Yu V Dubrovskiĭ, A Veretennikov, A Levin, A Patane, L Eaves, P C Main, M Henini, G Hill

Quantum dots (QD) make up nanostructures in which electron motion is restricted in the three spatial directions. This leads to a series of discrete energy levels for the electrons in quantum dots, similar to the case of an atomic spectrum. In the last few years the energy spectra of the quantum dots that form in the process of growing strained epitaxial InAs layers by the Stranski – Krastanov method have been studied in various ways [1], but so far no experimental studies of the spatial distribution of the electron wave functions in InAs quantum dots have been conducted. Although scanning tunnel spectroscopy makes it possible to obtain an image of the electron distribution at (or near) the surface of a heterostructure [2], quantum dots are often located far from the surface. In the report we show how magnetotunneling spectroscopy can be used as a nondestructive method that makes it possible to experimentally extract information about the probability density distribution of the electron wave function in self-assembled quantum dots (SAQD) [3].

The samples used in the experiments were AlGaAs/GaAs double-barrier heterostructures with a thin InAs film at the center of the GaAs quantum well [1.8 and 2.3 monolayers (ML)]. The InAs self-assembled quantum dots form in the process of growing strained epitaxial InAs layers by the Stranski – Krastanov method. Substrates with surface orientations (311)B and (100) were used in growing the heterostructure by the molecular beam epitaxy (MBE) method. The differences in growth conditions for the strained InAs layers and in the substrate orientations led to differences in shape and size of the emerging quantum dots and hence to differences in their energy spectra. In addition, reference structures without InAs layers were used. Selective *n*-doping made it possible to create junctions from above and from the substrate side. The standard technology of chemical etching was employed to create a mesoscopic structure 20 – 100 μm in diameter (Fig. 1a).

The photoluminescence spectra of the samples grown on the substrates with (100) and (311) orientations and thicknesses of the InAs layers amounting to 1.8 and 2.3 ML as well as of samples grown on substrates with the (100) orientation

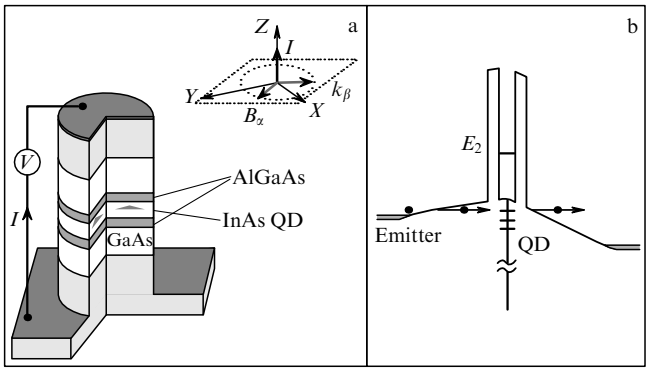

Figure 1. (a) Schematic of AlGaAs/GaAs resonance tunnel diode with a InAs self-assembled quantum dot at the center of a GaAs quantum well. Inset: mutual orientation of the magnetic field B and current I. X and Y are the principal crystallographic axes, α and β specify, respectively, the direction of B and of the electron momentum acquired, due to the Lorentz force, during tunneling. The pyramids depict the orientation of the quantum dot with respect to the coordinate axes. (b) Profile of the bottom of the conduction band.

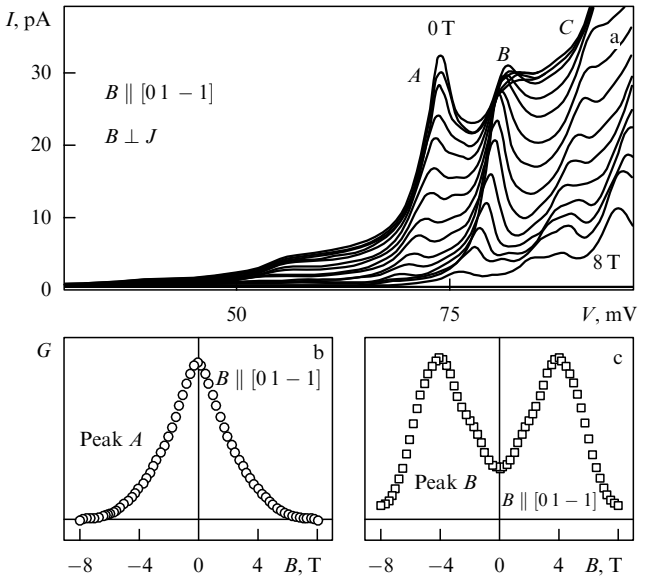

Figure 2. (a) Low-temperature ($T = 4.2$ K) current – voltage characteristics $I(V)$ in the presence of a magnetic field. The magnetic field strength changes from 0 to 8 T with a 0.5-T increment. The magnetic field B is perpendicular to the electric current. (b) and (c) The magnetic field dependence of the differential conductance, $G(B) = \mathrm{d}I/\mathrm{d}V$, with the magnetic field parallel to the [01 − 1] axis for different states of the quantum dots.

and the thickness of the InAs layer amounting to 1.8 ML exhibited a line with an energy of 1.27 – 1.35 eV, corresponding to the photoluminescence of InAs quantum dots. The characteristic size of the quantum dots (~ 20 nm) and the dot number density (0.5×10^{11} cm^{-2}) were determined by the scanning tunnel spectroscopy for samples grown in the same conditions as those under investigation. Transverse transmission electron microscopy (TTEM) was used directly to study a sample grown for tunnel transport measurements. The height of the dot was found to be about 2 – 3 nm.

The bottom profile of the conduction band of our heterostructure is depicted in Fig. 1b. The InAs layer of self-assembled quantum dots forms a set of electron states below the bottom of the conduction band in the GaAs quantum well. Some of these states are filled by electrons even under a zero bias, and in the region adjacent to the AlAs barriers these form a depleted layer. When a bias voltage is applied, tunneling through the discrete electron states leads to peaks in the current – voltage characteristics $I(V)$. These characteristics were measured by the standard direct-current method with a noise current less than 50 fA. The measurements were carried out in the 4.2 – 100-mK temperature range in magnetic fields of the induction up to 12 T.

We studied tunneling through InAs quantum dots in a magnetic field directed lengthwise of the growth plane (X, Y), i.e. perpendicular to the current. Below we shall consider samples grown on a (311)B substrate. In this plane, the principal crystallographic axes are [01−1] and [−233]. The results obtained for samples grown onto a (100) substrate are similar.

Figure 2a depicts the low-temperature ($T = 4.2$ K) current – voltage characteristics $I(V)$ in the presence of a magnetic field B. This magnetic field lies in the (X, Y) plane and is perpendicular to the electric current (see the inset to Fig. 1a). The [01−1] and [−233] axes determine the two principal crystallographic axes in the plane perpendicular to the direction of growth, [311]. The amplitude of each resonance strongly depends on the magnetic field strength. In particular, as B increases, the amplitude of the peak A decreases, while the amplitudes of the peaks B and C exhibit a nonmonotonic dependence on the magnetic field strength. Figures 2b and c clearly show two characteristic types of the magnetic-field dependence. Notice that all the resonances are suppressed in high magnetic fields.

But if at a certain fixed magnetic field strength the orientation of the magnetic field with respect to the principal crystallographic axes in the (X, Y) plane is varied, the amplitudes of the peaks begin to exhibit a strong dependence on this orientation (Fig. 3a), and the minima and maxima in the angular dependences of amplitudes of all the observed resonances for samples grown onto (311) substrates coincide, to within $\sim 15°$, with the principal crystallographic axes in this plane (Fig. 3b).

We can explain the magnetic-field dependence of the resonance amplitudes through examining the effect of the magnetic field on the tunneling electron. Let α, β, and z denote, respectively, the direction of B, the direction perpendicular to B in the growth plane (X, Y), and the direction perpendicular to the (X, Y) plane. When an electron tunnels from the emitter into the quantum dot in a magnetic field, it acquires an additional momentum $\Delta k_\beta = eB\Delta S/\hbar$, where ΔS is the effective tunneling length along z [4] (the momentum in the direction β changes due to the Lorentz force acting on the tunneling electron).

Applying a bias voltage to the heterostructure makes it possible to lower the energy of states of the quantum dots with respect to the emitter's Fermi energy and to observe peaks (when the energies coincide) in the current, corresponding to tunneling through these states at the quantum dot. Then, measuring the variation of the tunnel current caused by the variation of B, we can determine the value of the matrix element that describes the electron's transition from the emitter to the quantum dot. In our experiment we found it convenient to express the matrix element of the tunnel transition in terms of the Fourier transforms of the electron wave functions $\Phi_{i(f)}(k)$, where i and f correspond to the initial

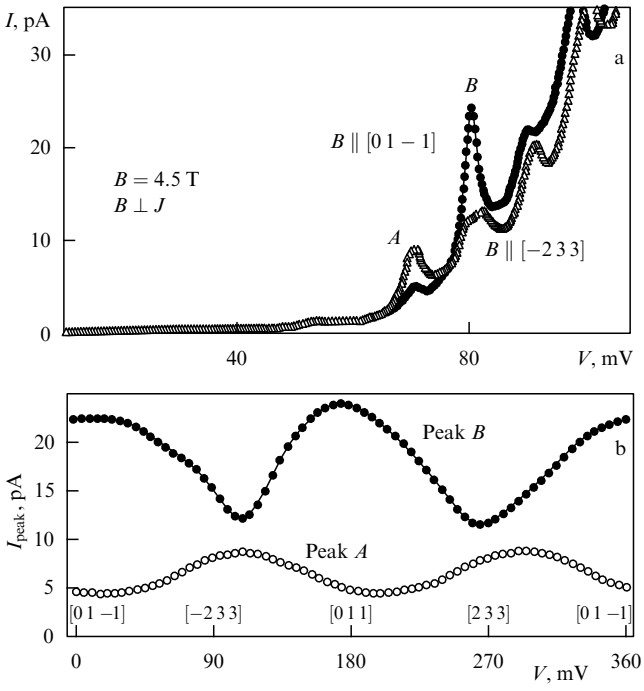

Figure 3. (a) Current–voltage characteristics $I(V)$ for the case of a magnetic field $B = 4.5$ T that is perpendicular to the electric current. The first curve (small black disks) represents the case where $B||[-1\ -1]$, and the second curve (small open triangles) represents the case where $B||[-233]$. (b) Angular dependence of the peak currents for the resonances A and B.

(emitter) and final (quantum dot) states between which the tunnel transition occurs [5, 6]. Note that the initial states of the emitter are rather weakly localized in the real space, in contrast to the strongly localized states of quantum dots. Hence $\Phi_i(k)$ in the k-space is represented by a Dirac delta function, which is nonzero only in the vicinity of $k = 0$. And since the tunnel current is determined by the square of the matrix element which contains both $\Phi_i(k)$ and $\Phi_f(k)$, the fact that $\Phi_i(k)$ is a Dirac delta function makes it possible to determine the shape of the function

$$\Phi_f(k) = \Phi_{QD}(k)\,,$$

by varying B and hence k. Thus, in reality, by measuring the dependence $I(B)$ [or $G(B)$] for a certain direction of B, we can find the shape of $|\Phi_{QD}(k)|^2$ along the direction of k perpendicular to B. Then, rotating B in the (X, Y) plane and measuring $I(B)$ (in a sequence) for different orientations of B, we obtain the complete spatial profile of $|\Phi_{QD}(k_x, k_y)|^2$, which is the projection of the probability density of a given electronic state of the quantum dot in the k-space in the plane perpendicular to the current [3].

Figure 4 depicts the profiles of differential conductance

$$G(B) = \frac{dI}{dV} \sim \left|\Phi_{QD}(k_x, k_y)\right|^2$$

in the (k_x, k_y) plane for the two quantum-dot states corresponding to Figs 3a, b. The resulting contour maps visualize the probability density distribution of the wave functions of the ground and excited states of a quantum dot. The electron wave functions are biaxially symmetric in the growth plane with the axes corresponding (to within measurement errors of about 15°) to the principal crystallographic

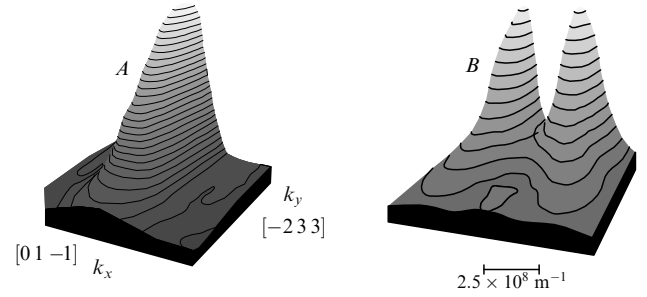

Figure 4. Profiles of the differential conductance, $G(B) = dI/dV \sim |\Phi_{QD}(k_x, k_y)|^2$, in the ($k_x$, k_y) plane for the two states of the quantum dots, corresponding to Figs 3a, b. The contour maps visualize the probability density distribution of the wave functions of the ground and excited states of a quantum dot.

directions X and Y for a (311) substrate orientation. For a (100) substrate we also obtained the characteristic images of the probability density for the ground and excited SAQD states.

The main result of the present work is a method that makes it possible to extract experimental information about the probability density distribution of the wave functions of electrons in self-assembled quantum dots. So far the proposed method is the only nondestructive technique for creating maps of the wave functions in SAQDs and has been applied to the given class of problems for the first time.

This work was made possible by grants from the Russian Foundation for Basic Research (grants 00-02-17903 and 01-02-17844), the Physics of Solid Nanostructures Program (97-1057), INTAS–RFBR (2000-774), and EPSRC (UK). The authors are grateful to V A Tulin and V G Lysenko for fruitful discussions and interest in the work, and to V V Belov and A Orlov for helping with the experiments.

References

1. Bimberg D, Grundmann M, Ledentsov N N *Quantum Dot Heterostructures* (New York: John Wiley, 1999)
2. Topinka M A et al. *Science* **289** 2323 (2000)
3. Vdovin E E et al. *Science* **290** 122 (2000)
4. Hayden R K et al. *Phys. Rev. Lett.* **66** 1749 (1991)
5. Beton P H et al. *Phys. Rev. Lett.* **75** 1996 (1995)
6. Sakai J-W et al. *Phys. Rev. B* **48** 5664 (1993)

PACS numbers: 71.45.Gm , 71.55.Eq , 73.20.Mf , 73.40.Gk

DOI: 10.1070/PU2001v044n12ABEH001056

Tunneling spectroscopy of quasi-two-dimensional plasmons

V A Volkov, É Takhtamirov, D Yu Ivanov, Yu V Dubrovskiĭ, L Eaves, P C Main, M Henini, D K Maude, J-C Portal, J C Maan, G Hill

1. Introduction

In two-dimensional (2D) electron systems based on semiconductors with an isotropic, parabolic dispersion law, the electron motion along the interface and transverse to the interface separates. Hence, in a magnetic field B that is

perpendicular to the interface, the one-particle Landau levels (LL) from different subbands do not interact with each other, and crossing of these levels is possible [1]. The situation is quite different with 2D systems based on semiconductors with a highly nonparabolic spectrum, such as the narrow-gap semiconductor PbTe [2]. Tunnel measurements in the latter case demonstrate anticrossing of Landau levels belonging to different 2D subbands.

We were the first to discover the strong interaction between such Landau levels in a tunnel 2D system based on GaAs, which is a semiconductor with an almost perfect parabolic dispersion law for the electrons. Highly disordered samples were used in the experiments, which made it possible to resolve the tunnel transitions between two 2D systems with and without a change of the LL number in the $2D \rightarrow 2D$ tunneling process.

2. Measurements

2.1 Samples

We used a single-barrier $GaAs/Al_{0.4}Ga_{0.6}As/GaAs$ heterostructure with a barrier 12-nm thick and vertical tunnel transport. The barrier was separated from the highly doped junction regions by undoped spacers 50-nm thick. To form the 2D electron layers, we employed delta-doping with silicon with a concentration in each layer amounting to 3×10^{11} cm^{-2} at a distance of 5 nm on each side of the barrier. Wet etching was used to form mesoscopic structures 100 – 400 μm in diameter. The penetrability of the tunnel barrier was much lower than that of the spacer, whereby almost the entire voltage applied to the structure falls on the tunnel barrier. Measurements of Shubnikov – de Haas type oscillations of the tunnel current yielded a value of electron concentration in the 2D layers approximately equal to the value of the concentration of the doping impurity. A schematic of the band diagram for the structure under investigation is depicted in Fig. 1 for a zero bias voltage. A typical value of the electron mobility amounted to $\mu = 1000$ cm^2 V^{-1} s^{-1} at 4.2 K.

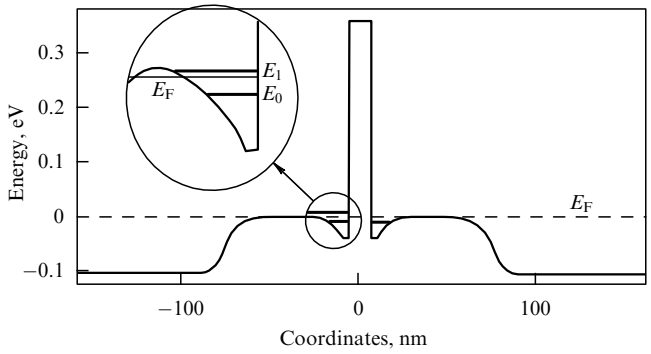

Figure 1. Schematic band diagram for a zero bias voltage. The inset shows the energy levels in 2D systems in greater detail: E_0 and E_1 are the bottoms of the ground and first excited 2D subbands, and E_F is the Fermi energy.

2.2 Experiment

Figure 2 depicts the differential tunneling conductivity G at 4.2 K (measured by the standard lock-in method) as a function of the applied bias voltage V_b in different magnetic fields up to 15 T. In a zero magnetic field (the lower curve in Fig. 2), the differential conductivity has a peak at zero bias voltage and two prominent 'arms' at higher bias voltages for both polarities of the applied voltage. The peak at zero bias voltage reflects the resonance nature of the tunneling between the ground states of the right and left electron systems, while the 'arms' appear because of resonance tunneling between the ground 2D subband ($n = 0$) of the emitter system and the first excited subband ($n = 1$) of the collector system. The very fact that there is a prominent peak in zero magnetic field and at zero bias voltage indicates that the fraction of tunneling processes proceeding with the conservation of momentum along the interface is relatively large, despite the large number of scattering centers. The development of these singularities as the magnetic field strength grows is due to tunneling between different Landau levels.

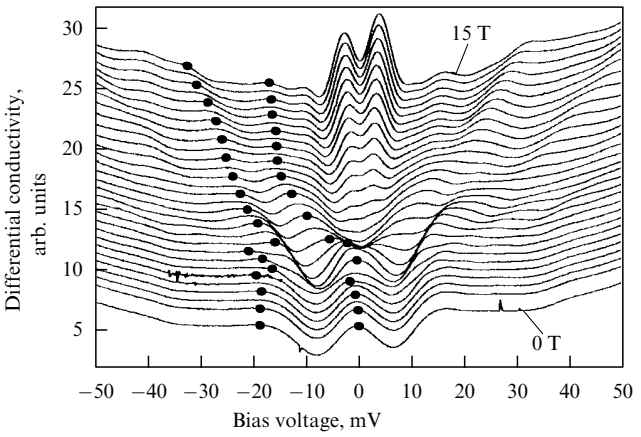

Figure 2. Differential tunneling conductivity at 4.2 K as a function of the bias voltage applied to the structure for a mesoscopic structure 400 μm in diameter. The lower curve corresponds to the case where $B = 0$ T. The second curve from below was measured at $B = 1$ T. All the other curves correspond to magnetic field induction increments by $\Delta B = 0.5$ T up to $B = 15$ T. The peaks whose evolution is discussed in the present work are marked by small black disks.

In the vicinity of $B = 6$ T, i.e. near an LL filling factor $\nu = 2$, the measured $G(V)$ curves demonstrate (see Fig. 2) a sizable minimum for a zero bias voltage. A further increase in B gradually transforms the minimum into two maxima. A detailed discussion of the tunneling process in the vicinity of zero bias voltage can be found in Ref. [3] and will not be discussed here.

3. Results

Let us discuss the behavior of the 'arms' in the $G(V)$ dependence, which are indicated by small black disks in Fig. 2. The fan-shaped diagram for such transitions is depicted in Fig. 3. Here we consider only negative bias voltages, since the main features of this diagram are symmetric in voltage.

In magnetic fields higher than 12 T and for bias voltages in the vicinity of 30 mV, the small dark disks correspond to a transition between the lower Landau level ($N = 0$) of the ground 2D subband ($n = 0$) in the emitter and the first excited Landau level ($N = 1$) of the ground 2D subband ($n = 0$) in the collector, i.e. $(n = 0, N = 0) \rightarrow (n = 0, N = 1)$. The dashed straight line A has a slope $L\hbar\omega_c$, where ω_c is the cyclotron frequency, and $L = 1.28$ is the electrostatic factor (the ratio of the applied voltage to the voltage falling on the barrier). This

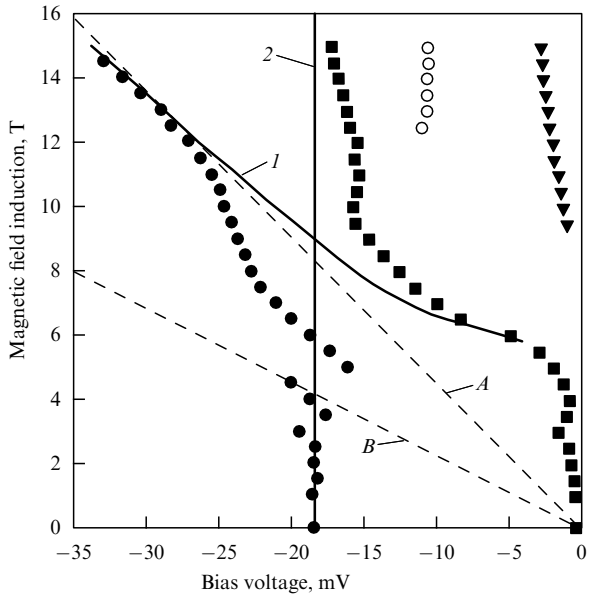

Figure 3. Position of peaks on the bias voltage scale as a function of magnetic field induction. The circles, squares, and triangles represent experimental data and their meaning is discussed in the text. Curve *1* displays the calculated position of the peak in the $(n = 0,\ N = 0) \to (n = 0,\ N = 1)$ transition, where N is the LL number. The vertical line labelled *2* represents the expected position of the peak in the $(n = 0,\ N = 0) \to (n = 1,\ N = 0)$ transition. Neither curve takes into account the interaction between the Landau levels. The straight lines *A* and *B* have slopes $L\hbar\omega_c$ and $2L\hbar\omega_c$, respectively, and describe tunneling between Landau levels with $\Delta N = 1$ and $\Delta N = 2$, where $L = 1.28$.

line demonstrates the position of the peak for tunneling with $\Delta N = 1$ in an approximation that ignores the broadening of the Landau level. The dashed straight line *B* represents (in the same approximation) the position of peaks for tunneling with $\Delta N = 2$.

For broadened Landau levels, the measured differential tunneling conductivity is determined by the density of states at the Fermi level in the emitter 2D system. The calculated positions of the peaks for transitions $(n = 0,\ N = 0) \to (n = 0,\ N = 1)$ between broadened Landau levels is depicted by the solid curve *1*. The position of the peaks corresponding to tunneling with LL number conservation ($\Delta N = 0$) does not depend on the magnetic field intensity and must coincide with the vertical straight line *2*. When there is no interaction between the Landau levels, some of the lines in Fig. 3 should cross, as lines *1* and *2* do. Instead there appears distinct repulsion of the lines consisting of dark disks and squares, which proves the Landau levels $(n = 0,\ N = 1)$ and $(n = 1,\ N = 0)$ interact. The observed splitting is about 10 meV. A certain indication that there is line repulsion can also be seen in the vicinity of the point of crossing of lines *2* and *B*, which corresponds to interaction of the Landau levels $(n = 0,\ N = 2)$ and $(n = 1,\ N = 0)$ in the collector system. Unfortunately, the accuracy of determining the position of the peaks is not high enough to make more specific statements.

To make the picture complete, we also depict the positions of the peaks in the vicinity of zero bias voltage (the triangle-based curves), which have been described by Khanin et al. [3], who studied the tunneling energy gap at the Fermi level in a magnetic field. The origin of the peaks represented by the open circles near 14 mV in magnetic fields higher than 12 T is apparently related to the spin splitting in the system under consideration.

4. Possible reasons for anticrossing

Let us discuss the possible reasons for the strong ($\sim$ 10 meV) anticrossing of the levels $(n = 0,\ N = 1)$ and $(n = 1,\ N = 0)$ observed in our experiments. The mechanism responsible for this effect must mix the longitudinal (along the layer) and transverse (perpendicular to the barrier) electron motions in the quasi-two-dimensional (Q2D) system.

4.1 Misorientation of magnetic field

Experiments in an oblique magnetic field have shown that the precision with which the magnetic field was oriented along the current ($\mathbf{B} \parallel \mathbf{J}$) was sufficiently high to exclude the effect of the magnetic field's component in the sample plane on anticrossing. More exactly, a misorientation ($\mathbf{B}$ and $\mathbf{J}$) of about 5° had no noticeable effect on the pattern in Fig. 3, and there were no noticeable quantitative changes either.

4.2 Nonparabolicity of the electronic spectrum $E(k)$

Another possible reason for anticrossing could be the nonparabolicity of the electronic spectrum $E(k)$ in GaAs. Qualitatively similar anticrossing has been observed in the highly nonparabolic material PbTe [2]. However, in the case of PbTe the strong anticrossing of Landau levels is caused by the fact that the principal axes of the constant-energy ellipsoids of the bottom of the conduction band (the L-points of the Brillouin zone) do not coincide with the direction of growth. This is not true of GaAs, and estimates of the contribution of this effect (nonparabolicity) to anticrossing yield a value of order 1 meV, which is too small to explain the detected effect.

4.3 Tunneling with participation of magnetoplasmons

An alternative explanation of anticrossing is based on collective excitations of the electronic system. Let us discuss the possible mechanisms of energy relaxation of an electron that has tunnelled onto an excited level in a system with a totally discrete spectrum. It is a common fact that if the distance to a low-lying level is an integral multiple of the LO-phonon energy, then the energy relaxation occurs due to resonance emission of such phonons. This corresponds to the appearance of phonon replicas in the tunneling spectrum. In our case such processes are still forbidden (phonon replicas are observed at much higher bias voltages V_b). On the other hand, relaxation accompanied by emission of Q2D magneto-plasmons with a characteristic energy equal either to $\hbar\omega_c$ (intrasubband plasmons) or the distance between the 2D subbands (intersubband plasmons [4]) is allowed in energy. Generally speaking, tunneling processes accompanied by resonance emission of intra- and intersubband 2D magneto-plasmons must manifest themselves in experiments in a way similar to single-particle processes in which the quantum numbers n and N change. The situation is quite different in the vicinity of the point of crossing of the single-particle terms *1* and *2* in Fig. 3. One should expect the Coulomb interaction, which is responsible for the emergence of plasma excitations, to lead to a strong interaction of the two magnetoplasmon branches mentioned earlier precisely in the vicinity of the point where the single-particle terms cross. This fact could be used to explain the observed anticrossing of 'single-particle' terms.

Now we turn to a quantitative description of the spectrum of Q2D magnetoplasmons. There exist a large number of theoretical studies devoted to the plasmon spectrum in Q2D systems. In most of these the plasmons were investigated in the absence of a magnetic field (e.g. see Refs [4–6]). The researchers found that there are two plasmon branches: intrasubband plasmons related to electron oscillations in the ground 2D subband, and intersubband plasmons related to virtual transitions between 2D subbands. The first have a gapless spectrum, while the second exhibit a weak dispersion and a gap with a width equal to the sum of the intersubband energy Δ and the depolarization energy. The interaction of intersubband and intrasubband modes in the absence of a magnetic field is extremely weak even for a specially selected geometry of the structure [7]. A number of papers have been devoted to calculating the spectrum of Q2D plasmons in a magnetic field (e.g. see Refs [8–11]). The results contain an extremely rich structure of the spectrum of such magnetoplasmons but very strongly depend on the approximations employed and the type of a system. We calculated the magnetoplasmon spectrum in the random phase approximation for the structure studied in our experiment. Since plasmons are excited in the process of 2D $\rightarrow$ 2D tunneling in the symmetric system, only antisymmetric (with respect to the barrier's center) plasmon modes are of interest. The result was obtained in the dipole approximation [small wave vectors $\mathbf{q} = (q_x, q_y)$] for fairly strong magnetic fields, when the filling factor is $\nu < 4$.

Our finding is depicted in Fig. 4, where four magnetoplasmon branches are shown, namely, the intersubband branch *1*, the intrasubband branch *2*, and the combined resonance branches *3* and *4* related to virtual transitions between the states $(n = 0, N = 1)$ and $(n = 1, N = 0)$ as well as $(n = 0, N = 0)$ and $(n = 1, N = 1)$. The depolarization energy in this case is close to 4 meV. At $q = 0$, the magnetoplasmon energies coincide with the energies of single-particle excitations depicted in Fig. 4 by lines consisting of small open circles and crosses. Possibly, it was the anticrossing of the branches *1* and *4* that was discovered in our experiments due to the high density of states on these branches. The observed anticrossing of the two peaks can be interpreted as relaxation on 'hybrid' intra- and intersubband magnetoplasmons. The unusual shape of the anticrossing in Fig. 3 is, possibly, related to the effect of branch *2* in Fig. 4.

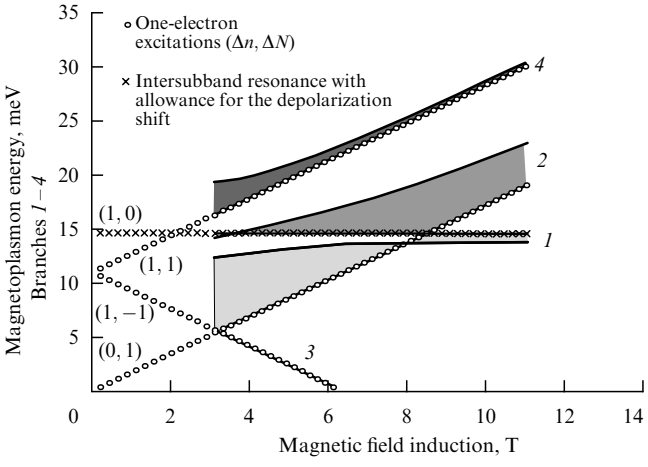

Figure 4. Magnetoplasmon energy (four branches) as a function of magnetic field induction for different wave vectors q. The shaded regions correspond to values of q ranging from zero to 5×10^5 cm^{-1}. Branch *1* represents an intersubband plasmon, branch *2* an intrasubband plasmon, and branches *3* and *4* represent plasmons of a combined resonance with transitions $\Delta - \omega_c$ and $\Delta + \omega_c$, respectively. Lines consisting of small open circles indicate the energy of single-particle excitations $(\Delta n, \Delta N)$; $\Delta = 11$ meV is the intersubband energy.

5. Conclusions

We have studied tunneling between highly disordered 2D electron systems in a quantized magnetic field parallel to the current. A strong interaction between the Landau levels belonging to different 2D subbands has been discovered. We proposed an explanation for the observed anticrossing related to the excitation of intra- and intersubband magnetoplasmons in a Q2D system.

This work was made possible by support given by the Russian Foundation for Basic Research (projects 99-02-17592, 01-02-97020, and 01-02-06476), the Physics of Solid Nanostructures Program, the Surface Atomic Structures Program, and the Physics of Quantum and Wave Processes Program.

References

1. Duke C B *Phys. Rev.* **159** 632 (1967); Ben Daniel D J, Duke C B *Phys. Rev.* **160** 679 (1967); Duke C B *Phys. Lett. A* **24** 461 (1967); Baraff G A, Appelbaum J A *Phys. Rev. B* **5** 475 (1972)
2. Tsui D C, Kaminsky G, Schmidt P H *Phys. Rev. B* **9** 3524 (1974)
3. Khanin Yu N et al. *Physica E* **6** 602 (2000)
4. Dahl D A, Sham L J *Phys. Rev. B* **16** 651 (1977)
5. Vitlina R Z, Chaplik A V *Zh. Eksp. Teor. Fiz.* **81** 1011 (1981) [*Sov. Phys. JETP* **54** 536 (1981)]
6. Jain J K, Das Sarma S *Phys. Rev. B* **36** 5949 (1987)
7. Hu C-M, Schüller C, Heitmann D *Phys. Rev. B* **64** 073303 (2001)
8. Chiu K W, Quinn J J *Phys. Rev. B* **9** 4724 (1974)
9. Tselis A, Quinn J J *Surf. Sci.* **113** 362 (1982)
10. Wendler L, Pechstedt R *J. Phys.: Condens. Matter* **2** 8881 (1990)
11. Bisti V E *Pis'ma Zh. Eksp. Teor. Fiz.* **69** 543 (1999) [*JETP Lett.* **69** 584 (1999)]

PACS numbers: **73.61.–r**, 85.30.Vw, 85.30.Tv

DOI: 10.1070/PU2001v044n12ABEH001057

Quantum dot Ge/Si heterostructures

A V Dvurechenskiĭ, A I Yakimov

1. Introduction

Determining the parameters of the energy spectrum, the kinetics of the transitions between electronic states, and the interaction of elementary excitations and establishing the correlation effects constitute the basis for current fundamental research in the field of quantum dots (QD). Among the numerous heterostructures with quantum dots (see Refs [1–4]) that are being actively studied the silicon-based structures have always provoked special interest, due to the promising integration of the results of such research and the basic silicon technology used in building modern semiconductor devices and circuits. The substantial advances in the epitaxy of Ge on Si and the prospects for using Ge/Si heterostructures formed the natural basis for systems with quantum dots. From the viewpoint of fundamental research,

the Ge/Si system form type-II heterostructures. In such systems the localized states for electrons and holes are formed on different sides of the interface in self-consistent potential wells. The electrons and holes in such states are spatially separated, and a transition between these states is indirect in space.

In this report we present some of the data on the electronic properties of the QD array in germanium that forms on the Si(100) surface due to the effect of spontaneous morphological transformation of an elastically strained Ge layer grown in MBE conditions and then overgrown by a Si layer. In the first papers devoted to the study of such structures we discovered the Coulomb-blockade and size-quantization effects in the hole energy spectrum [5, 6]. We also found the conditions needed for low-temperature heteroepitaxy to be carried out, conditions that lead to the formation of nanometer-size islands with a surface density of $(3-5)\times10^{11}$ cm^{-2} [3]. The average size of Ge clusters shaped as pyramids was 15 nm (the pyramid's base), the pyramid height was 1.5 nm, and the spread of sizes was no greater than 17%.

2. Energy spectrum of hole states

In the Ge/Si system with Ge clusters, the relative arrangement of the energy bands forms a potential well only for holes. The geometry of the germanium island leads to a great difference between the size-quantization energy in the base plane of the pyramid and that in the direction of growth (the pyramid height is much smaller than the base size). Since the symmetry of the problem is close to that of a disk, the ground energy level corresponds to an *s*-shaped state, and the first excited level to a *p*-shaped state. Calculations have shown that the difference in the energies of the *s* and *p* states is quantized in the pyramid's base plane [7]. Thus, optical transitions between the given states are possible if the light is polarized in the pyramid's base plane (under normal incidence of the light onto the structure, which is especially important for practical implementations).

Electron spectroscopy studies of QD arrays of Ge in Si have shown that the hole state spectrum is discrete. What makes this type of QD array special is that the average cluster size is comparable to the cluster separation (a dense array). In such a system, the size quantization energy E_q and the Coulomb interaction energy E_c are of the same order, in contrast to the large clusters often described in the scientific literature, in which $E_c \gg E_q$ [1]. In dense QD arrays, both the interaction of carriers inside a single dot and the interaction with the surroundings contribute to E_c, as distinct from the case of a rarefied array, where the interaction with the surroundings can be ignored. The data gathered by different methods suggest that for the selected Ge/Si object with quantum dots one obtains $E_q \approx 75$ meV (the distance between the ground and first excited states on the energy scale). The energy of the ground state (measured from the top of the valance band in Si) is in the 405–430-meV energy range, and E_c is approximately 36 and 18 meV for the ground state (two holes) and the first excited state (four holes), respectively. The smaller value of E_c for the excited state is due to the larger value of the hole localization radius: 7.6 nm for the ground state, and 15.0 nm for the excited state. When these states are occupied, the contribution to E_c from the interaction of holes inside a single quantum dot amounts to 11 meV for the ground state and 5.4 meV for the excited state [8, 9].

3. Energy structure of excitons and exciton complexes

In conditions where the hole density in the QDs is zero (the QDs are occupied with electrons), optical transitions of electrons from the QD to the Si conduction band become possible [9, 10]. The formation of an exciton corresponds to a Gaussian-shaped absorption band with the peak at 770 meV and a width of 50 – 70 meV, apparently caused by the Ge cluster shape and size fluctuations. The energy of electron localization near the Ge/Si interface proved to be approximately 30 meV, the oscillator strength f was 0.5, and the band-to-band absorption cross section was 2.5×10^{-16} cm^2. The last value is more than 10 times the typical photoionization cross section for deep level impurities in Si. The value of f is approximately 20 times smaller than the oscillator strength for direct excitons in the InAs/GaAs system, where $f = 10.9$, which is a direct consequence of the spatial separation of an electron and hole in the Ge/Si system (a type-II heterostructure).

An analysis carried out in the self-consistent field approximation with allowance for inhomogeneous elastic strains has shown that during exciton formation in the Ge/Si system with quantum dots the electron is localized in the vicinity of the vertex of the Ge pyramid (where the stresses are at their maximum in Si), while the hole is localized near the pyramid's base (see Fig. 1). The main contribution to the energy of electron localization at the Ge/Si interface is provided by the electron–hole Coulomb interaction

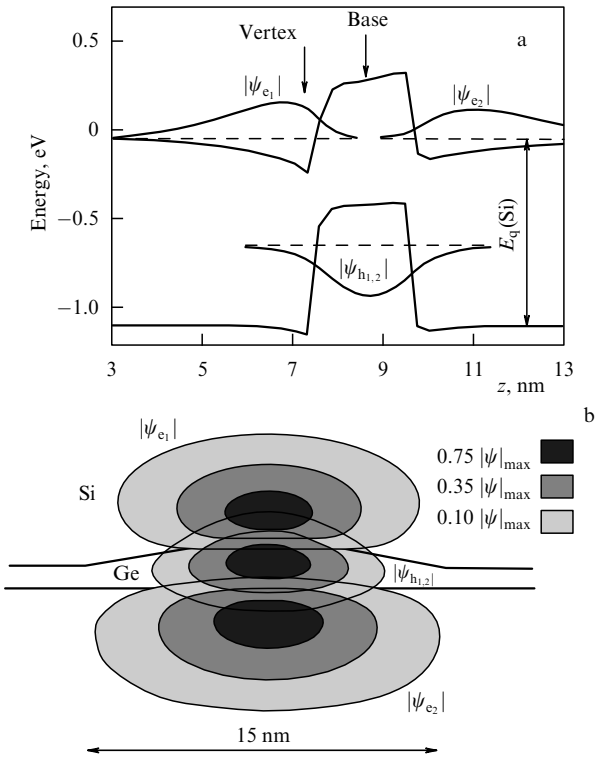

Figure 1. (a) Calculated profile of the potential, in which the electrons and holes constituting an exciton complex move, along the *z*-axis passing through the Ge pyramid vertex. (b) Two-dimensional image of the moduli of the electron $|\psi_e|$ and hole $|\psi_h|$ wave functions in the transverse section of a quantum dot and its surroundings. The degree of occupancy corresponds to regions at the boundaries of which the wave functions fall off to levels amounting to 75%, 35%, and 10% of the maximum value [10].

(28 meV). The contribution of the inhomogeneous strain distribution to potential-well formation amounts to 9 meV. In a complex consisting of two excitons, electron repulsion leads to their spatial separation, as a result of which the second electron proves to be bound at the boundary between Si and the continuous Ge layer on which the pyramids are arranged.

It has been established that the formation of charged exciton complexes (two holes – one electron) and exciton – exciton complexes in type II QDs leads to a shift in the exciton absorption energy into the short-wave region. This blue shift for charged complexes is caused by the spatial separation of electrons and holes in type II QDs, as a result of which the Coulomb interaction between the two holes in a QD dominates the electron – hole interaction. In a biexciton, the electrons are localized in different places in space, and the second electron is localized in a shallower potential well than the first. Thus, the biexciton's short-wave line shift is due to the difference in the energies of electron size quantization in different potential wells.

When a Ge/n-Si structure with quantum dots is illuminated by light that causes band-to-band transitions, negative photoconductivity comes into play. This is, probably, due to the trapping of electrons into states in the potential well formed at the interface of Ge/Si by nonequilibrium holes in Ge nanoclusters [11].

4. Interlevel optical transitions in quantum dots

In the particular case of a quantum well with a parabolic potential, the energy of an optical transition between subbands depends neither on the number of electrons in the well nor on the electron – electron interaction and is equal to the size quantization energy [12, 13]. For a nonparabolic potential and also when the contribution of the Coulomb interaction between quantum dots is substantial, the optical transition energy may differ substantially from the size quantization energy. The reason for this lies in the formation of collective oscillations in the system initiated by an incident electromagnetic wave (the depolarization effect observed in two-dimensional systems). Since the discovery of quantum dots (in which charge carrier motion is limited in all three dimensions), the question arose as to whether there exist collective effects in growth-plane-polarized optical transitions. Theoretical estimates have shown that a depolarization shift of the optical resonance can be observed when the layer concentration of the carriers is higher than 10^{11} cm^{-2}. In this sense our Ge/Si system with a dense QD array was an ideal object for establishing the presence of collective effects in interlevel optical transitions. Studies of the optical transitions between the levels in quantum dots in the Ge/Si system in the 70 – 90-meV energy range revealed an absorption maximum corresponding to a hole transition from the ground state to an excited one [10, 14]. The oscillator strength of such a transition amounted to 0.95, and the absorption cross section to 8×10^{-16} cm^2. A much smaller magnitude (1.6×10^{-16} cm^2) for interlevel hole transitions was obtained earlier for the InAs/GaAs system with quantum dots. It was found that at a small degree of occupancy of Ge quantum dots, the width of the absorption line is determined by the size variance of the nanocrystallites. The discovered shift of the absorption line into the short-wave region, the narrowing of the line, and changes in the line shape brought on by the increase in hole concentration in the ground QD state are characteristic manifestations of the depolarization effect.

5. Devices with built-in QD layers

The silicon field-effect transistors with a built-in germanium quantum dot layer contained, under the gate, from 10^3 (the size of the subgate region was about 1×1 μm^2) to 10^9 quantum dots [8]. The transistor channel and source – drain regions were boron doped, so that when the bias voltage across the gate was zero the channel conductivity was high. As the gate voltage became positive and grew, the conductivity exhibited a sharp drop (to zero at low temperatures), which was due to the formation of a depletion region. A further increase in the bias voltage was found to result in well-resolved current peaks related to hole transport through the discrete states in the quantum dots (Fig. 2). A decrease in the area of the region under the gate (a decrease in the number of quantum dots) allows one to observe the source – drain current oscillations as a function of the gate voltage at higher measurement temperatures (up to room temperatures). These data suggest that the Ge/Si heterostructures with a built-in QD layer are a promising material for building one-electron transistors.

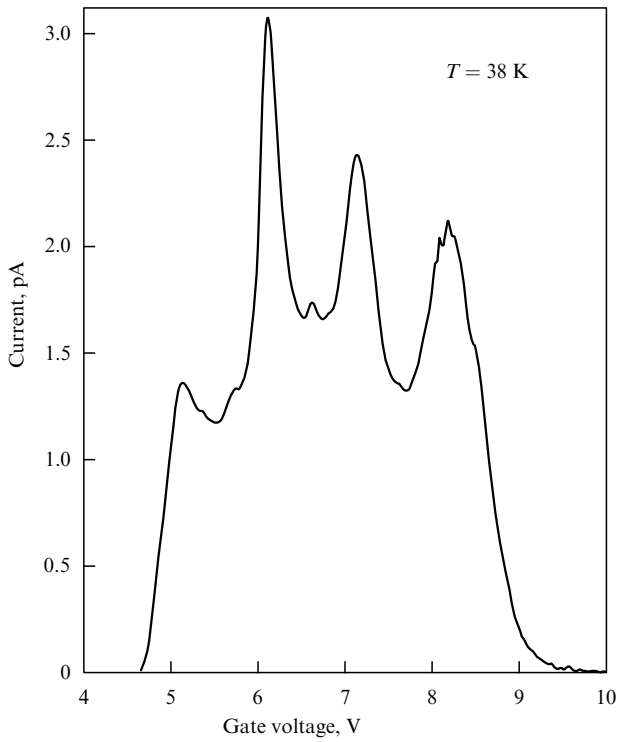

Figure 2. Source – drain current as a function of gate voltage in a field-effect transistor with 10^3 Ge quantum dots below the gate.

Studies of photoconductivity in Ge/Si structures with a built-in QD layer have revealed the possibility of creating photodetectors with a tunable spectral response. The maximum detectivity of a Ge/Si structure with quantum dots acting as a photodetector was 1.7×10^8 cm Hz$^{1/2}$ W^{-1} at a wavelength of 20 μm, and 0.7×10^8 cm Hz$^{1/2}$ W^{-1} at a wavelength of 10 μm at 300 K [15].

This work was made possible thanks to the support provided by the Physics of Solid Nanostructures Program (projects 98-1100 and 00-17-2F) and the Russian Foundation for Basic Research (projects 99-02-39051GFEN and 00-02-17885).

References

1. Jacak L, Hawrylak P, Wojs A *Quantum Dots* (Berlin: Springer-Verlag, 1998)
2. Ledentsov N N et al. *Fiz. Tekh. Poluprovodn.* **32** 385 (1998) [*Semiconductors* **32** 343 (1998)]
3. Pchelyakov O P et al. *Izv. Ross. Akad. Nauk Ser. Fiz.* **63** 228 (1999) [*Bull. Russ. Acad. Sci. Ser. Phys.* **63** 191 (1999)]
4. Vostokov N V et al. *Fiz. Tekh. Poluprovodn.* **34** 8 (2000) [*Semiconductors* **34** 6 (2000)]
5. Yakimov A I et al. *Philos. Mag. B* **65** 701 (1992)
6. Yakimov A I et al. *J. Phys.: Condens. Matter* **6** 2573 (1994)
7. Dvurechenskiĭ A V, Nenashev A A, Yakimov A I, in *Nanofotonika: Materialy Vseros. Soveshchaniya* (*Nizhniĭ Novgorod, Mart 2001*) [Nanophotonics: Proc. National Workshop (Nizhniĭ Novgorod, March 2001)] (Nizhniĭ Novgorod: IFM RAN, 2001)
8. Dvurechenskiĭ A V, Yakimov A I *Izv. Ross. Akad. Nauk Ser. Fiz.* **64** 288 (2000) [*Bull. Russ. Acad. Sci. Ser. Phys.* **64** 233 (2000)]
9. Dvurechenskiĭ A V, Yakimov A I *Izv. Ross. Akad. Nauk Ser. Fiz.* **65** 187 (2001) [*Bull. Russ. Acad. Sci. Ser. Phys.* **65** 205 (2001)]
10. Yakimov A I et al. *Zh. Eksp. Teor. Fiz.* **119** 574 (2001) [*JETP* **92** 500 (2001)]
11. Yakimov A I et al. *Phys. Rev. B* **62** R16283 (2000)
12. Wixforth A et al. *Phys. Rev. B* **43** 10000 (1991)
13. Sundaram M et al. *Appl. Phys. Lett.* **65** 2226 (1994)
14. Yakimov A I et al. *Phys. Rev. B* **62** 9939 (2000)
15. Yakimov A I et al. *J. Appl. Phys.* **89** 5676 (2001)

PACS numbers: 03.75.Fi, 71.35.Lk, 71.35.Ji

DOI: 10.1070/PU2001v044n12ABEH001058

Exciton Bose condensate control and the phonon laser

Yu E Lozovik

There exists a fruitful analogy between a system of quasi-particles, electrons and holes in excited semiconductors, on the one hand, and a system of 'true particles', electrons and protons (or, in a more general case, positive ions), on the other, since the laws of interaction in these systems are the same. The systems differ dramatically in the corresponding scales: the effective Bohr radius for excitons, which may be much larger than the Bohr radius, the exciton binding energy Ry*, which is much lower than the binding energy of the hydrogen atom, etc. This analogy opens an enticing possibility not only of predicting as yet undetected phases of the electron–hole system but, on the contrary, to model (via the electron–hole system) various phases of particle systems in extreme cosmological conditions [1], unattainable in laboratory experiments, in particular, in ultrahigh magnetic fields (e.g. for the detection of the anisotropic phase of polymer chains consisting of electric quadrupoles of atoms or excitons, extended along the magnetic field, or for magnetic dissociation and transformation of the type of molecular or excitonic bonds in ultrahigh magnetic fields, and so forth).

This analogy really exists. Indeed, the quasi-particle analogs of molecules are biexcitons, those of clusters are small electron–hole drops, and that of the liquid phase is the electron–hole liquid. The possibility of other phases is also being discussed.

However, there are important differences between these systems. Electrons and holes, in contrast to particles, usually 'exist' in an anisotropic (and largely 'random', due to defects) world of semiconductors and are often characterized by a complex (multivalley) dispersion law. This can lead to a phase diagram differing from that for a system of electrons and protons (e.g. stabilizing the metallic liquid phase, the electron–hole liquid [2]). Another bare parameter, the ratio of the masses of the positive and negative charges, also plays an important role: it controls the contribution of the zero-oscillation energy and determines whether there exists a crystalline phase as yet undetected in an electron–hole system.

In view of the amazing achievements in the technology of fabricating quite perfect nanostructures there has emerged another remarkable possibility, namely, to control the effective dimensionality and even the topology of the space where the quasi-particles 'exist'. This possibility broadens the variety of phase states and kinetic properties of the systems consisting of electrons and holes.

An interesting system in this respect is the quasi-two-dimensional system of spatially separated electrons and holes in coupled quantum wells [3] or the similar one-dimensional system in coupled quantum wires or in the zero-dimensional system of coupled quantum dots [4]. The quasi-zero-dimensional situation is also realized in an electron–hole system residing either in a single quantum well or in coupled quantum wells in quantizing magnetic fields [5–7] (however, the effective dimensionality in an interacting e–h system may depend on the occupancy of the Landau level).

When discussing the above systems with different dimensionalities, it must be kept in mind that here one is actually dealing with two radically different physical realizations.

The first realization corresponds to electrons and holes in a semiconductor's excited state that is generated, for instance, by laser radiation and exists over intervals shorter than the recombination times. The latter may be significantly increased, for instance, by virtue of a weak overlapping of the wave functions of the spatially separated electrons and holes in coupled quantum wells, and so on. This fact favors the possibility of establishing a partial thermodynamic equilibrium in the system and observing the different phase states of the electron–hole system in coupled quantum wells [3–13] (for similar phases in a three-dimensional system see Ref. [14]).

The second physical realization corresponds to an equilibrium system of spatially separated electrons and holes in coupled type II quantum wells (such a system in the coherent phase may manifest, due to particle tunneling through potential barriers between wells, several effects similar to the Josephson effect; see Ref. [15]).

I believe that there is one more system of keen interest: the disbalanced steady-state system of two identical coupled electron layers in a strong magnetic field [6]. The 'disbalance' of the two layers is achieved by applying a voltage V between them. Suppose that at $V = 0$ the two layers entirely fill a single (zeroth) Landau level. Then there is a system of excess electrons on the first Landau level in one layer and an equal number of unfilled positions (holes) on the zeroth Landau level in the other layer (or, when the disbalance is great, the electrons and holes are in different layers on the same Landau level). A situation that is even more curious

occurs when there is a small disbalance near a fractional occupancy of a Landau level. In this case there emerges a two-layer system of equilibrium electrons and holes with fractional charges.

Another interesting physical realization of the spatially separated electron – hole system is the electron system of two coupled quantum wells (or a double quantum well) placed in a strong transverse magnetic field, which resides in states with half-filled Landau levels in each layer. In each of these layers (when the hybridization between them is not too strong), the two-dimensional Fermi surface for quasi-particles (composite fermions) consisting of electrons with two attached flux quanta is 'restored' [16] (the shape of this surface is identical to that of the initial surface [17] in the absence of field).

Pairing of electrons and holes in all the above situations leads to a coherent phase that exhibits superfluid properties [3, 6, 8], specific optical properties (see Ref. [18] and the references cited therein), and Josephson type effects [15].

In recent experiments researchers observed intriguing optical phenomena that probably point to the presence of a coherent exciton phase [19, 20] (see also Refs [21, 22]). One would like, however, to analyze such optical effects that would suggest a coherent exciton phase not only quantitatively but also qualitatively, i.e. in a more unambiguous manner. Effects of this sort constitute the topic of the present report.

First, examples of such phenomena are the unusual stimulated two-photon emission and Raman scattering of light by two-dimensional Bose-condensed excitons, with the processes accompanied by coherent recombination or generation of two (overcondensate) excitons with opposite momenta [18]. Such stimulated two-photon emission and Raman scattering can be shown to be related to the emergence of spectral lines at frequencies $|\omega_0 \pm 2\Omega| - m\omega^s$, where ω_0 is the incident photon frequency, and ω^s is the frequency of a photon whose parallel momentum (in the quantum well plane) coincides with momentum of the lowest-energy exciton.

The intensity of these lines depends on the anomalous averages, with the result that these processes make it possible to directly study off-diagonal order and occur only if there is an exciton Bose condensate in the system. Hence they can be used for detecting a Bose condensate of excitons (or a 'quasi-condensate' in a two-dimensional system at $T \neq 0$). Numerical estimates have shown that the effect associated with these processes can be used to detect Bose condensation of spatially indirect excitons in a system of coupled AlAs/GaAs quantum wells.

Another vivid manifestation of exciton Bose condensation is a new optical phenomenon — stimulated back reflection of light in the case of (oblique) incidence of a laser beam onto a quasi-two-dimensional or semi-infinite exciton condensate [23]. The effect is caused by light-induced coherent recombination of two excitons from the Bose condensate, accompanied by the production of two photons with oppositely directed momenta. What is remarkable is that for a Q2D coherent system of excitons, in addition to the ordinary transmitted beam, there appears an anomalously transmitted beam whose direction is mirror-symmetric to that of the incident beam (see Fig. 1). It is interesting that these effects must also be present in a Bose condensate of excited Bose atoms (e.g. first cooled and then resonantly excited).

Note that in the absence of an incident laser beam two-exciton recombination leads to luminescence with a correlation between photon states with oppositely directed

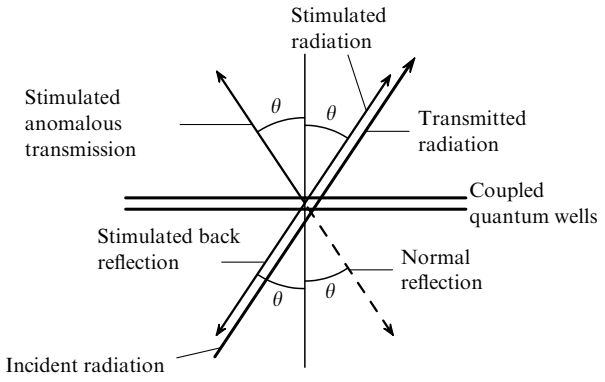

Figure 1.

momenta. Such a correlation can be detected in Hanbury – Braun – Twiss type experiments with two detectors placed on opposite sides of the exciton system.

Let us discuss in greater detail the possibility of controlling an exciton Bose condensate through the use of external fields and the phonon spectroscopy of the exciton Bose condensate.

In direct gap semiconductors, spatially indirect excitons in coupled quantum wells are direct excitons in the momentum space. Due to the weaker Coulomb attraction of an electron and hole, their level is above the level of a spatially direct electron. Since spatially indirect excitons have an electric dipole moment eD normal to the well plane, when an electric field E normal to the well plane is applied, splitting takes place, and the lower level shifts downward as eDE.

But a moving indirect exciton (an electric dipole eD) generates a magnetic moment $eDkh/(cM)$ in the quantum well plane, where k is the exciton momentum, and M is the exciton mass. When a magnetic field H is applied parallel to the quantum wells, there emerges an interaction (linear in the momentum k) between the magnetic moment and the magnetic field. Since this interaction is added to the exciton's quadratic dispersion law, it leads to a shift (sideways) in the dispersion law of the indirect exciton, and this shift is proportional to H. The shift can be interpreted differently, namely, as a manifestation of diamagnetism of the two-layer e – h system, i.e. the generation of currents flowing in opposite directions in the magnetic field parallel to the layers. This latter phenomenon corresponds to exciton motion (in the ground state) in the direction perpendicular to the field H [3, 15].

The displacement of the exciton's dispersion transforms the exciton into an indirect one in the momentum space and brings the exciton out of the radiation zone where recombination of the exciton accompanied by emission of a photon is possible: the exciton is transformed from 'light' to 'dark'. The described dispersion law engineering of spatially indirect excitons by means of applying a magnetic field parallel to the layers has been observed in the experiments described in Ref. [24].

The simultaneous control by an electric field E normal to the wells and a parallel magnetic field opens up even more remarkable possibilities. As noted earlier, an electric field shifts the energy level of indirect excitons. Hence it can be used to tune to resonance the recombination of indirect excitons via the level of spatially direct excitons through emission of an acoustic phonon, i.e. to the resonance of the

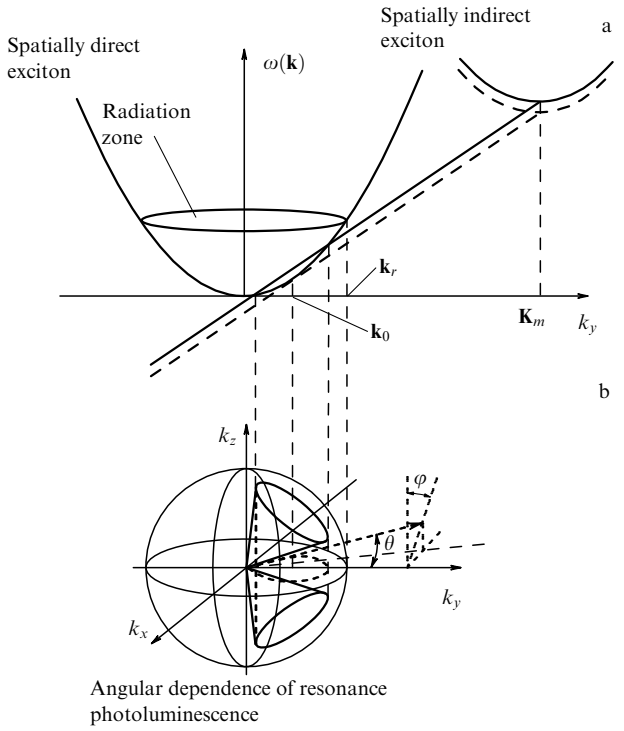

Figure 2.

process

indirect exciton → direct exciton + acoustic phonon.

In the process of tuning to resonance, the intensity of photoluminescence of the exciton condensate increases by several orders of magnitude and, as analysis of the laws of conservation of energy and momentum in the well plane shows, photoluminescence radiation turns out to be narrow-directed: it constitutes two oppositely directed beams propagating in the well plane (see Fig. 2). At the same time, the intensity of the phonon radiation also sharply increases, with this radiation forming a narrow beam, too. Furthermore, as shown by the analysis of the equation for the density matrix describing the photon and phonon generation process and of the integrals of motion for this equation, in realistic conditions the phonon radiation 'inherits', so to say, the statistics of the emitter, i.e. the system of indirect excitons [23]. This opens the possibility of phonon spectroscopy of an exciton Bose condensate. Moreover, the statistics of the phonons emitted by a (quasi-) condensate of indirect excitons is that of laser radiation, i.e. a phonon laser is realized. Clearly, the resonant process

indirect exciton → direct exciton + acoustic phonon

corresponds to the standard three-level lasing scheme with phonons acting as photons. Hence readily follow the conclusions concerning the attainability of conducting pulsed and continuous-wave operations for the phonon laser considered.

If there is a cavity for the phonons, phonon lasing is also achieved, naturally, through the use of an incoherent source (in our case, the source is a system of indirect excitons in an incoherent state), i.e. in the ordinary way, due to self-organization. In this connection I would like to point out some other possible schemes for a phonon laser. One is based on the employment of an indirect-narrow-gap semiconductor in which the gap is tuned (by applying pressure or a magnetic field) to resonance with a one-phonon emission [25].

Another possibility consists in the use of a scheme similar to the Capasso cascade laser, i.e. a superlattice of identical quantum wells manufactured from indirect-gap semiconductors and placed in an electric field such that the shift of the adjacent transverse quantization level is equal to the acoustic phonon energy.

This research was supported by grants from the Russian Foundation for Basic Research, INTAS, and the Physics of Solid Nanostructures Program.

References

1. Ginzburg V L *O Fizike i Astrofizike* (Key Problems of Physics and Astrophysics) (Moscow: Nauka, 1974)
2. Keldysh L V, in *Electron-Hole Liquid* (Amsterdam: North-Holland, 1986); Brinkman W F, Rice T M *Phys. Rev. B* **7** 1508 (1973)
3. Lozovik Yu E, Yudson V I *Pis'ma Zh. Eksp. Teor. Fiz.* **22** 26 (1975) [*JETP Lett.* **22** 11 (1975)]; *Zh. Eksp. Teor. Fiz.* **71** 738 (1976) [*Sov. Phys. JETP* **44** 389 (1976)]; *Solid State Commun.* **18** 628 (1976); **21** 211 (1977); *Physica A* **93** 493 (1978)
4. Lozovik Yu E, Verzakov S A, Willander M *Phys. Lett. A* **260** 400 (1999); Kaputkina N E, Lozovik Yu E *Phys. Status Solidi B* **221** 341 (2000)
5. Lerner I V, Lozovik Yu E *Zh. Eksp. Teor. Fiz.* **80** 1488 (1981) [*Sov. Phys. JETP* **53** 763 (1981)]; *Zh. Eksp. Teor. Fiz.* **82** 1188 (1982) [*Sov. Phys. JETP* **55** 691 (1982)]; *Zh. Eksp. Teor. Fiz.* **78** 1167 (1980) [*Sov. Phys. JETP* **51** 588 (1980)]; Dzyubenko A B, Lozovik Yu E *Fiz. Tverd. Tela* (Leningrad) **25** 1519 (1983); **26** 1540 (1984) [*Sov. Phys. Solid State* **25** 874 (1983); **26** 938 (1984)]; *J. Phys. A* **24** 415 (1991); Paquet D, Rice T M, Ueda K *Phys. Rev. B* **32** 5208 (1985)
6. Lozovik Yu E, Berman O L, Tsvetus V G *Phys. Rev. B* **59** 5627 (1999); Lozovik Yu E, Ruvinskiĭ A M *Zh. Eksp. Teor. Fiz.* **112** 1791 (1997) [*JETP* **85** 979 (1997)]
7. Yoshioka D, MacDonald A H *J. Phys. Soc. Jpn.* **59** 4211 (1990); Yoshioka D, Fukuyama H *J. Phys. Soc. Jpn.* **50** 725 (1978)
8. Lozovik Yu E, Berman O L *Pis'ma Zh. Eksp. Teor. Fiz.* **64** 526 (1996) [*JETP Lett.* **64** 573 (1996)]; *Zh. Eksp. Teor. Fiz.* **111** 1879 (1997) [*JETP* **84** 1027 (1997)]; Ivanov L N, Lozovik Yu E, Musin D R *J. Phys. C* **11** 2527 (1978); Lozovik Yu E, Berman O L, Willander M *Zh. Eksp. Teor. Fiz.* **115** 1786 (1999) [*JETP* **88** 980 (1999)]; Lozovik Yu E, Berman O L, Ruvinskiĭ A M *Pis'ma Zh. Eksp. Teor. Fiz.* **69** 573 (1999) [*JETP Lett.* **69** 616 (1999)]
9. Zhu X et al. *Phys. Rev. Lett.* **74** 1633 (1995)
10. Conti S, Vignale G, MacDonald A H *Phys. Rev. B* **57** R6846 (1998)
11. Schmitt-Rink S, Chemla D S, Miller D A B *Adv. Phys.* **38** 89 (1989)
12. Chen X M, Quinn J J *Phys. Rev. Lett.* **67** 895 (1991)
13. Bauer G E W *Phys. Scripta T* **45** 154 (1992)
14. Keldysh L V, Kopaev Yu V *Fiz. Tverd. Tela* (Leningrad) **6** 2791 (1964) [*Sov. Phys. Solid State* **6** 2219 (1964)]; Keldysh L V, Kozlov A N *Zh. Eksp. Teor. Fiz.* **54** 978 (1968) [*Sov. Phys. JETP* **27** 521 (1968)]; Kozlov A N, Maksimov L A *Zh. Eksp. Teor. Fiz.* **48** 1184 (1965) [*Sov. Phys. JETP* **21** 790 (1965)]; Halperin B I, Rice T M *Solid State Phys.* **21** 115 (1968); Lozovik Yu E, Yudson V I *Fiz. Tverd. Tela* (Leningrad) **17** 1613 (1975); Keldysh L V, in *Bose–Einstein Condensation* (Eds A Griffin, D W Snoke, S Stringari) (Cambridge: Cambridge Univ. Press, 1995) p. 246
15. Klyuchnik A V, Lozovik Yu E *Zh. Eksp. Teor. Fiz.* **76** 670 (1979) [*Sov. Phys. JETP* **49** 335 (1979)]; *J. Low Temp. Phys.* **38** 761 (1980); *J. Phys. C* **11** L483 (1978); Lozovik Yu E, Yudson V I *Pis'ma Zh. Eksp. Teor. Fiz.* **25** 18 (1977) [*JETP Lett.* **25** 14 (1977)]; Shevchenko S I *Phys. Rev. Lett.* **72** 3242 (1994); Lozovik Yu E, Yudson V I *Solid State Commun.* **22** 117 (1977); Lozovik Yu E, Poushnov A V *Phys. Lett. A* **228** 399 (1997)
16. Halperin B I, Lee P A, Read N *Phys. Rev. B* **47** 7312 (1993)
17. Balagurov D B, Lozovik Yu E *Phys. Rev. B* **61** 1481 (2000)
18. Lozovik Yu E, Poushnov A V *Phys. Rev. B* **58** 6608 (1998); Lozovik Yu E, Pushnov A V *Zh. Eksp. Teor. Fiz.* **115** 1353 (1999) [*JETP* **88** 747 (1999)]; Lozovik Yu E (to be published)
19. Butov L V, Filin A I *Phys. Rev. B* **58** 1980 (1998)
20. Larionov A V et al. *Zh. Eksp. Teor. Fiz.* **117** 1255 (2000) [*JETP* **90** 1093 (2000)]; *Pis'ma Zh. Eksp. Teor. Fiz.* **71** 174 (2000) [*JETP Lett.* **71** 117 (2000)]; **73** 342 (2001) [*JETP Lett.* **73** 327 (2001)]

21. Fukuzawa T, Mendez E E, Hong J M *Phys. Rev. Lett.* **64** 3066 (1990)
22. Cheng J-P et al. *Phys. Rev. Lett.* **74** 450 (1995)
23. Lozovik Yu E, Ovchinnikov I V *Solid State Commun.* **118** 2519 (2001)
24. Butov L V et al. *Phys. Rev. B* **62** 1548 (2000)
25. Lozovik Yu E, Merkulova S P, Ovchinnikov I V *Phys. Lett. A* **282** 407 (2001)

PACS numbers: 29.25.Bx, 29.27.Hj, 79.60.Jv
DOI: 10.1070/PU2001v044n12ABEH001058

Effective polarized electron emitters based on semiconductor nanostructures

A V Subashiev

High-energy beams of spin-polarized electrons have proven to be exceptionally useful in many experiments of elementary particle physics. By studying the scattering of polarized electrons by polarized and unpolarized targets it is possible to restore what is known as the nucleon spin structure functions and to investigate problems associated with the relative contribution of quarks and gluons to the observed value of nucleon spin, problems whose solutions are important for the development of quantum chromodynamics [1].

The second direction of research in this field is the study of CP symmetry violation in the electroweak interaction. The main result here is the exceptional accuracy (the relative error is about 0.1%) in measuring the electroweak mixing angle [2]. These measurements allowed the making of the most stringent (for the present) estimate of the maximum possible value of the Higgs boson mass. The value of 147 GeV c^{-2} obtained in this estimation was found to be within the range of energy attainable for modern accelerators, which makes the hope of discovering this particle in the near future quite realistic.

Less intensive is the expansion of polarized electron beam applications in materials science and, in particular, when investigating spin-dependent scattering, inverse photoemission, and spin-dependent absorption in thin films and surface layers of magnetic and semimagnetic materials [3].

The main achievements in the development and use of sources of highly polarized electrons have been made in the last decade, beginning with the experimental research in photoemission from highly strained semiconducting InGaAs and GaAs layers [4, 5], in which the possibility of creating a 75–85% electron polarization was demonstrated for the first time. Since that time semiconductor photocathodes with strained layers became the standard sources of electron beams in accelerators. Their main merit is the possibility of rapidly and precisely changing the orientation of the electron spin to the opposite, which makes it possible to specify the spin-dependent part of cross sections with ease.

The degree of the electron polarization of a beam determines the accuracy of measuring the spin-dependent effects, especially in the cases where there are limitations on the electron beam current, which are related to the properties of the target. The polarization of nearly 80% in the region of the targets is sufficiently high for the majority of experiments. A further increase in polarization and current density in the beam would make it possible to shorten the measurement times and would therefore reduce the cost of such experiments.

The development of research that uses the beams of polarized electrons has stimulated the study of polarized photoemission and the fabrication of new semiconducting materials with optimal photoemissive properties. In this report I will discuss the results and prospects of such research.

The operation of semiconductor photoemitters of polarized electrons leans upon two phenomena well-known in physics of semiconducting III–V compounds: optical orientation of electron spins as a result of excitation by circularly polarized light [6], and reduction of the work function of a p-doped semiconductor to negative electron affinity (when the vacuum level is below the edge of the conduction band in the crystal) in the process of activation of an atomically clean surface by a Cs(O) [or Cs(F)] deposition [7]. Here photoemission appears to be a consequence of the following processes: interband light absorption, trapping of electrons to the region of band bending at the surface (this region emerges because of the pinning of the Fermi level at the surface states within the forbidden band), and emission proper, i.e. the tunneling from the near-surface well into the vacuum through the residual surface barrier.

Such a pattern has been corroborated by experiments and calculations of the photoemission excitation spectra, the spectra of the energy distribution of the emitted electrons, and the dependence of these spectra on the photoemitter parameters (such as the doping level, layer thickness, temperature, and so forth) [3, 7].

Optical orientation is caused by the spin–orbit splitting of the valence band states, as a result of which the upper split-off states of the heavy and light holes have a total angular momentum $J = 3/2$ and are characterized by strong mixing of the orbital and spin movements. The difference between the probabilities for optical transitions to the conduction band from states of the multiplet with angular momentum projections $J_z = \pm 3/2$ and $J_z = \pm 1/2$, which are accompanied by the electron angular momentum change equal to unity (when the absorbed light is circularly polarized), results in unequal population of the two spin states of the conduction band: $|\uparrow\rangle$ and $|\downarrow\rangle$. The emerging optical orientation of the spins is characterized by the polarization $P = (n_\uparrow - n_\downarrow)/(n_\uparrow + n_\downarrow)$, where $n_\uparrow$, $n_\downarrow$ are, respectively, the concentrations of electrons with spins parallel and antiparallel to the direction of light propagation in the crystal [6].

Additional splitting of the multiplet with $J = 3/2$ into the subbands of heavy ($J_z = \pm 3/2$) and light ($J_z = \pm 1/2$) holes, when the crystal is under uniaxial strain, is used to make only one electron state populated. A fairly high strain is achieved by growing a $Ga_xIn_{1-x}As$ layer with a large lattice constant on a GaAs substrate. The best results have been achieved by growing GaAs (or $GaAs_{0.95}P_{0.05}$) layers on a $GaAs_xP_{1-x}$ (with $x = 0.28-0.32$) pseudosubstrate obtained, for instance, by growing a sequence of $GaAs_{1-y}P_y$ layers on a GaAs substrate with increasing concentration y. To reach the necessary photoemission current, the thickness of the photocathode's active layer must be no less than 0.1 μm, which is ten times the critical thickness for such strained layers and corresponds to dislocation-free growth. For this reason strained films prove to be partially relaxed and have a highly imperfect block crystalline structure. This in turn leads to a smearing of the absorption edge, hole scattering from defects in the process of absorption, and the filling of the second electron spin state, which reduces the initial polarization.

The above mechanism of polarization loss can be distinguished by calculating the dependence of the photoemission quantum yield Y and the polarization P of photoemission and photoluminescence radiations on the excitation energy and by

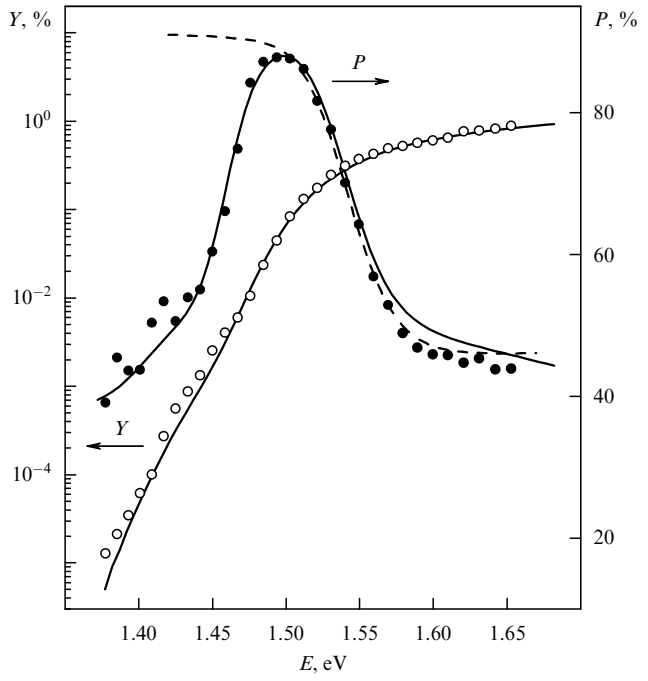

Figure 1. Degree of spin polarization P of photoelectrons and the photoemission quantum yield Y as functions of the excitation energy E for a strained GaAs film on a $GaAs_{0.72}P_{0.28}$ pseudosubstrate at $T = 300$ K; the experimental results and the results of calculations without allowance for smearing of the absorption edge (dashed curve) and with allowance for that smearing (solid curves) are depicted.

comparing the results to the experimental data (see Fig. 1) [8]. Calculations made it possible to determine the parameters of strained films (experimentally examined and calculated polarized luminescence excitation spectra were compared simultaneously to exclude any ambiguity in such a procedure). It was found that the initial polarization primarily depends on the ratio between the strain-induced valence-band splitting Δ_{str} and the parameters characterizing the smearing of the interband absorption edge due to indirect transitions in which optical phonons and tails of the density of states belonging to the valence band participate. The peak value of the electron polarization at the momentum of excitation is roughly 94% (for the given sample).

Additional depolarization occurs when electrons are extracted to the space charge region near the surface, which manifests itself in time-resolved experiments involving excitation by short pulses and also in experiments with films of different thicknesses. In thin films of thickness $d \ll L$, $1/\alpha$ (where L is the diffusion length, and α is the light absorption coefficient), the time of carrier trapping into the space charge region is $\tau_{esc} = d/S$, where S is the surface recombination rate. Here the decrease in the carrier polarization $\delta P = -d/(S\tau_s)$, where τ_s is the electron spin relaxation time in the active layer. For typical values of the layer parameters these losses amount to about 7% for $d = 100$ nm and decrease in lightly doped samples with lowering temperature.

Experimental studies of the dependences of polarized distribution functions on the energy of the escaped electrons indicate that there is a weak depolarization of electrons in the band bending region near the surface for energies below the bottom of the conduction band. In view of the spatial separation of carriers in this region, the main mechanism of spin relaxation is the precession of electron spins in the effective crystal field, whose magnitude and direction are determined by the magnitude and direction of the electron momentum (the D'yakonov–Perel' mechanism [6]). In the potential well of the band bending region there is a strong fluctuative Coulomb potential generated by ionized acceptors and donors, with states below the percolation level being localized in the surface plane. Electrons rapidly relax in energy, emitting optical phonons up to the percolation level, after which the D'yakonov–Perel' mechanism proves to be suppressed due to the averaging of the effective field over the directions of electron movements.

For this reason heavy doping of the band bending region does not lead to additional depolarization of the emitted electrons. This conclusion is especially important for emitters designed for generating high-density emission currents (≈ 1 A cm^{-2}), when due to intensive optical excitation there may be a buildup of electrons at the surface states and partial straightening of the surface band bending, which leads to a decrease in quantum yield. Heavy doping of the near-surface region suppresses these effects [9].

Analysis of the various mechanisms of spin polarization losses at the different stages of photoemission shows that these losses in strained films are close in magnitude, while the range of accessible variations of the layer parameters is quite narrow.

Semiconducting strained short-period superlattices constitute alternative materials for photocathodes. In such structures the splitting of the states in the valence band may be made much greater due to the difference in masses of heavy and light holes and their size quantization in layers corresponding to the quantum wells, and the initial polarization may be made much higher. Furthermore, one can use superlattices with a reduced average strain in the active area (when the wells are highly deformed), and therefore with a more perfect crystal structure. Finally, profile doping may easily be introduced into the technology of superlattice growth, which makes it possible to retain a high acceptor level only within a narrow layer near the surface and to increase the spin relaxation time in the active area.

An important advantage of superlattices is the large number of variable parameters, which allows the optimization of the structure in such a way so as to minimize polarization losses at each stage in photoemission without degradation of the emission properties, for instance, by reducing the average spin–orbit splitting while retaining a high spin–orbit splitting in the well materials.

So far the $In_xGa_{1-x}As/Al_yGa_{1-y}As$ and $GaAs/GaAs_yP_{1-y}$ superlattices with strained wells [3, 10] and $GaAs/Al_xIn_yGa_{1-x-y}As$ superlattices with strained barriers [11] have been studied. In the latter structure, the use of the quaternary composition in the barrier makes it possible to reduce the conduction band offset at heterointerfaces to a minimum. This ensures a high mobility of the electrons along the superlattice axis and reduces the polarization losses during extraction.

The employment of modulation doping in the $Al_xIn_yGa_{1-x-y}As/GaAs$ superlattice, in addition to high deformation of the layers, makes is possible to reliably achieve an 86% polarization (P) with a high quantum yield Y in the vicinity of the polarization peak. In less strained lattices, the polarization at a photoemission maximum proves to be smaller.

The problem of optimizing the photoemitter's structure is rather complicated, and its solution is only at the initial stage.

First we must know the band structure of the material and the spectrum of initial electron polarization and their dependences on the parameters of the materials of the layers and the structure as a whole. Calculations of the band structure, the absorption coefficient, and the degree of initial orientation of the electrons for superlattice-based photoemitters were first done in Ref. [12] in the multiband Kane model within the enveloping function approximation. The results of these calculations for a superlattice with strained barriers and the basic optical transitions corresponding to the strongest van Hove singularities in the interband absorption spectrum are depicted in Fig. 2.

The results of calculations of the polarization spectrum [12] for an energy separation of 37 meV between the hole subbands and a parameter γ that characterizes the smearing of the absorption edge and equals 10 meV are depicted in Fig. 3 (without corrections for spin relaxation under thermalization). The fairly good agreement with the experimental data indicates that it is possible to employ such calculations in optimizing photoemissive structures and in restoring the parameters of strained superlattices, in particular, the conduction band offset at heterointerfaces. The advantages of using polarized electrons are in many ways similar to those of harnessing polarized light in optics, for example, in Raman spectroscopy: the gain in information is worth the effort in developing the appropriate technology, which has been fully realized in high-energy physics. Undoubtedly, spectroscopy (including tunneling spectroscopy) and microscopy that use polarized electrons will develop rapidly in the near future.

The main obstacle to the wide harnessing of the existing photoemitters of polarized electrons in materials science is the high sensitivity of the Cs(O) [or Cs(F)] activation layer to the vacuum conditions (a fairly long lifetime of the activated surface is achieved at a residual pressure of $10^{-11}-10^{-12}$ Torr) and the relatively low sensitivity of the most common Mott polarimeters (combined with the low accuracy of such polarimeters). The progress in developing more stable activation layers, protective coatings, and membranes and in manufacturing new compact and sensitive polarimeters based on multilayer magnetic structures is sure to solve these problems.

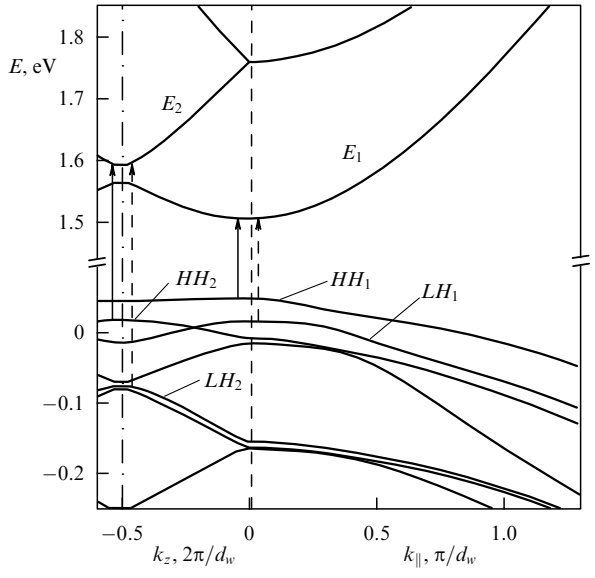

Figure 2. The band structure of the short-period strained GaAs/$Al_{0.18}In_{0.16}Ga_{0.66}As$ superlattice with equal barrier and well widths: $d_B = d_w = 4$ nm. The arrows indicate transitions that produce the principal singularities in the initial polarization spectrum.

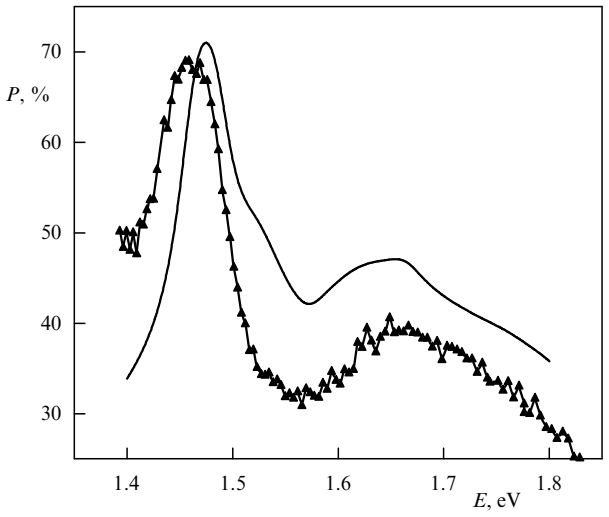

Figure 3. Spectral dependence of the photoemission spectra for a superlattice with the parameters specified in Fig. 2; the experimental results (triangles) and the results of calculating polarization at the moment of excitation (solid curve) are depicted.

A detailed investigation into the kinetics of polarized electrons in semiconductor nanostructures, the effects related to heterointerfaces, doping, and near-surface layers as well as the properties of these entities will be useful not only in developing new photoemissive materials but also in developing the elements of spin electronics.

This work was made possible thanks to the support provided by the Physics of Solid Nanostructures Program (project 97-1090) and INTAS (grant 99-00125) and the partial support of the Russian Foundation for Basic Research (project 00-02-16775).

References

1. *Proc. 14th Int. Spin Physics Symp.: SPIN 2000, Osaka, Japan, 2000* (AIP Conf. Proc., Vol. 570, Eds K Hatanaka et al.) (Melville, N.Y.: AIP, 2001)
2. Abe K et al. (SLD Collab.) *Phys. Rev. Lett.* **86** 1162 (2001)
3. Subashiev A V et al. *Phys. Low-Dim. Struct.* (1/2) 1 (1999)
4. Maruyama T et al. *Phys. Rev. Lett.* **66** 2376 (1991)
5. Nakanishi T et al. *Phys. Lett. A* **158** 345 (1991)
6. Maĭer F, Zakharchenya B P (Eds) *Opticheskaya Orientatsiya* (Optical Orientation) (Leningrad: Nauka, 1974) [Translated into English (Amsterdam: Elsevier Sci. Publ., 1984)]
7. Bell R L *Negative Electron Affinity Devices* (Oxford: Clarendon Press, 1973) [Translated into Russian (Moscow: Énergiya, 1978)]
8. Subashiev A V et al. *Fiz. Tekh. Poluprovodn.* **33** 1307 (1999) [*Semicond.* **33** 1182 (1999)]
9. Mulhollan G et al. *Phys. Lett. A* **282** 309 (2001)
10. Nakanishi T, in *Polarized Gas Targets and Polarized Beams, 7th Int. Workshop: Urbana, 1998* (AIP Conf. Proc., Vol. 421, Eds R J Holt, M A Miller) (Woodbury, N.Y.: AIP, 1998) p. 300
11. Subashiev A V et al., in *Proc. 24th Int. Conf. on Physics of Semiconductors (ICPS-24): Jerusalem, 1998*; see also Preprint, SLAC-PUB-7922 (Stanford, 1998)
12. Andreev A D, Subashiev A V, in *Proc. 9th Int. Symp.* "*Nanostructures: Physics and Technology*": *St.-Petersburg, June, 2001* (St.-Petersburg, 2001) p. 269